LOng-LIved greenhouse gas PrOducts Performances (LOLIPOP)

WP 7200 Consistent and improved N_2O profiles from IASI

TN-7.2 - Technical note on IASI NOPIR final improvements and reprocessed data

Document Reference	[D7.2] LOLIPOP_TN-7.2_v2.0
Document Authors	Sophie Vandenbussche (BIRA-IASB)
Document Approvers	S. Pinnock (ESA, Technical Officer)

Change log:

Version Nr.	**Date**	**Status**	**Reason for change**
Version 1.0	10/11/2025	Document creation	N/A
Version 2.0	15/05/2025	Document update	Adding information after full processing of IASI-A and IASI-C

Table of Contents

1 Introduction

1.1 Scope of the document

The Nitrous Oxide Profiling from Infrared Radiances (NOPIR) algorithm retrieves N_2O vertical profiles (with up to 2 degrees of freedom) from IASI satellite observations. The first version of the algorithm was a demonstration algorithm, used to produce a data time series from 2011 to 2020 and was shown very promising (Vandenbussche et al., 2022). However, the time series contained inconsistencies due to regular updates in the IASI level 2 data used as input for NOPIR.

This document contains the technical description of the IASI NOPIR algorithm improvement undertaken within LOLIPOP, including changes to obtain consistent N_2O data and further retrieval improvements.

1.2 Reference Document

[RD-1] LOLIPOP CCN Options proposal

1.3 Acronyms and Abbreviations

Abbreviation	Meaning
CAMEL	Combined ASTER and MODIS Emissivity database over Land
CCI	Climate Change Initiative
ECV	Essential Climate Variable
ESA	European Space Agency
IASI	Infrared Atmospheric Sounding Interferometer
LOLIPOP	Long Lived greenhouse gas PrOducts Performances
NOPIR	Nitrous Oxide Profiling from Infrared Radiances
OE	Optimal Estimation
PCS	Principal Components Scores
PWLR3	Piece-Wise Linear Regression version 3
RTTOV	Radiative Transfer for TOVS

2 The NOPIR algorithm and its improvements

2.1 Introduction

The NOPIR algorithm in his first version is fully described in Vandenbussche et al. (2022). The retrieval is based on the Tikhonov regularization scheme, uses selected IASI spectral micro-windows in the N_2O ν_3 band (between 2170 and 2215 cm^{-1}) and the Radiative Transfer for TOVS (RTTOV) tools. The initial validation showed a partial column (over the retrieval range) positive bias of maximum 4% with respect to ground-based observations from NDACC and TCCON networks. This bias is within the sum of uncertainties of the compared data sets.

However, the long-term series contain inconsistencies that are clearly related to updates in the IASI level 2 data, used as input for the NOPIR retrievals. At the time of the initial publication and data processing, no consistent IASI level 2 data existed. However, now fully consistent reprocessed IASI level 1 and level 2 data exist from EUMETSAT. This opened the path to obtaining NOPIR reprocessed and consistent data, taking also the opportunity to improve the algorithm and solve the detected issues.

In this document, we will not describe again the retrieval algorithm in detail, but we will clearly report all changes from version 1 to version 2, including changes to the input data.

2.2 Time-consistent IASI input data

EUMETSAT now provides reprocessed data for IASI-A (level 1 Principal Components Scores or PCS, and level 2 Piece-Wise Linear Regression version 3 or PWLR3), which is also consistent with the processing algorithm for IASI-C until March 2023 for the level 1 PCS and until at least mid-2025 for the level 2 PWLR3. Table 1 provides the detailed reference of those data sets.

Since 30 March 2023, a new eigenvector basis is used for the level 1 PCS creation. The IASI-C data series seems to remain fully consistent across this change, as no noticeable change is detected in the NOPIR time series.

In addition, with that new version of PCS comes the launch of the hybrid PCS that include also some local PCS and eigenvectors to better catch unexpected local spectral signatures that would not have been well represented in the global PCS and eigenvectors. We currently do not use those additional local PCS: the N_2O signature is well represented in the global eigenvector basis and is not expected to bear strong unusual local variations; therefore, we avoid unnecessary complications, data handling and potential discontinuity.

Table 1: EUMETSAT level 1 and level 2 data used in NOPIR v2

	IASI-A (2007-2021)	IASI-C (2019-now)
Level 1 Principal Components Scores	IASI Principal Components Scores Fundamental Data Record Release 1 - Metop-A and -B, European Organisation for the Exploitation of Meteorological Satellites, DOI: 10.15770/EUM_SEC_CLM_0084	IASI Level 1 Principal Component Scores - Metop – Global (EO:EUM:DAT:METOP:IASPCS01)
Level 2 PWLR3 T and H_2O profiles and cloud product	IASI All Sky Temperature and Humidity Profiles - Climate Data Record Release 1.1 - Metop-A and -B, European Organisation for the Exploitation of Meteorological	IASI Combined Sounding Products – Metop (Collection ID EO:EUM:DAT:METOP:IASSND02), from which we use the PWLR3 result (“first guess”) for T and H_2O profiles

	Satellites, DOI: 10.15770/EUM_SEC_CLM_0063	

Finally, let us note that the level 2 reprocessed data contain the results of only the first step (or so-called “first guess”) of the standard EUMETSAT level 2 retrieval: the PWLR3. The optimal estimation (OE) final step of the retrieval is not provided in the reprocessed data. The quality difference as assessed in the EUMETSAT documentation (EUMETSAT, 2021) is minimal, however there are still some differences in the NOPIR retrieval using the PWLR3 or OE level 2 input. Basic comparisons were done, and it was not possible to conclude which IASI level 2 data (OE or PWLR3) lead to the best NOPIR results. Using the PWLR3 data also for IASI-C is the only way to obtain time consistent data since the start of IASI observations, and it is therefore selected for NOPIR.

With this consistent data and NOPIR version 1 before any additional retrieval change, the expected time consistency in N_2O columns has been verified, processing only data around the previous inconsistencies (which were due to IASI algorithm updates). Figure 1 and Figure 2 clearly show that there is no more inconsistency when using the reprocessed IASI data as input for NOPIR.

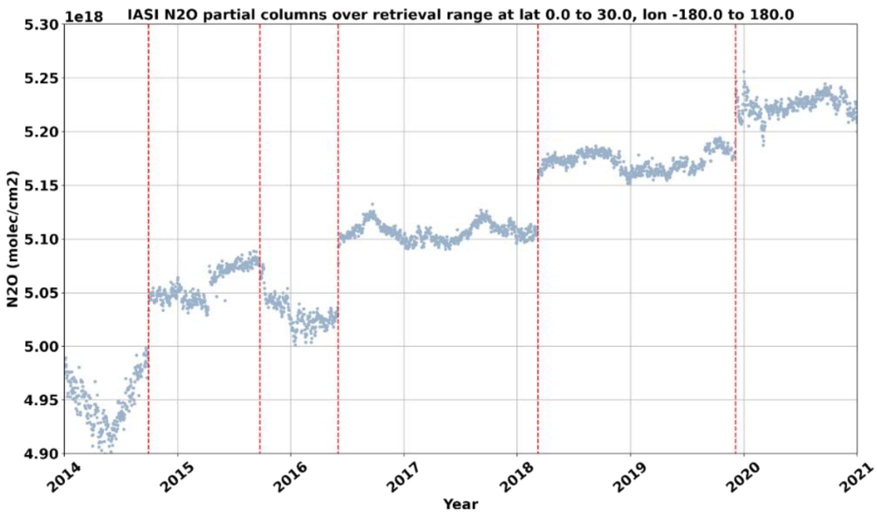

Figure 1: North Tropical (0-30°N) zonal mean of NOPIR version 1 N_2O column (800-80hPa) as a function of time, using the IASI near-real-time disseminated data as input

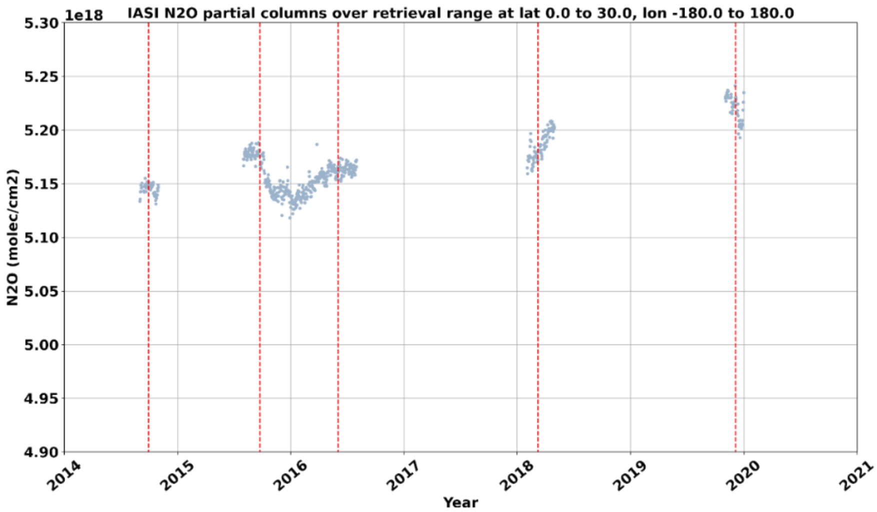

Figure 2: same as Figure 1 but using the reprocessed IASI data as input; only a limited data set was produced simply to verify the consistency

2.3 Quality control and filtering on input IASI data

Due to an update in the IASI data used as input for NOPIR, the quality filtering is also updated and therefore detailed here. The IASI-A and IASI-C data being different in terms of format and available flags, the filtering is also different but should not result in inconsistency in NOPIR outputs.

For each spectrum (PCS), the following criteria are applied:

<u>IASI-A:</u>

- in the spectral band used (B3): QFlag = 0 (this is a quality flag that integrates information from other flags, and it is only provided in the reprocessed data; its detailed description is not available and reproducing the exact filtering for IASI-C is therefore not feasible)

<u>IASI-C:</u>

- GQisQualIndex >= 95

- in the spectral band used (B3): GQisFlagQual = 0

- in the spectral band used (B3): ResidualRMS <= 1.5

If any of those criteria is not met, the spectrum is rejected. In addition, after spectrum reconstruction the radiances are checked and any NaN or negative value leads to rejection of the spectrum. This should however never occur.

For each set of level 2 profiles, the following criteria are applied, including the cloud filtering:

<u>IASI-A</u>

- qualityIndicatorForAtmosphericTemperature <= 2K

- qualityIndicatorForAtmosphericWaterVapour <= 5K

- FLG_IASIBAD = 0

- CloudFraction (in level 1 data) <= 10%

IASI-C

- FG_QI_ATMOSPHERIC_TEMPERATURE <= 2K

- FG_QI_ATMOSPHERIC_WATER_VAPOUR <= 5K

- FLG_IASIBAD = 0- GEUMAvhrr1BCldFrac (in level 1 data) <= 10%

If any of the criteria is not met, the IASI pixel is rejected. The complex cloud flag (FLG_CLDNES) was not used as it does not exist in the reprocessed data, and the cloud filtering should also be as consistent as possible between IASI-A and IASI-C.

In addition, all atmospheric profiles (pressure, temperature, water vapour) and the surface temperature and pressure must be within the acceptable boundaries for RTTOV version 14 (see table 7.7 in Hocking et al. 2025). Therefore, the atmospheric profile of water vapour is internally clipped (within RTTOV, this is an input parameter) to acceptable values (1e-11 to 60000 ppmv). The surface pressure and atmospheric profile of pressure and temperature cannot be corrected with sufficient certainty and are not retrieved in NOPIR. Given their impact on the retrieval results, if any of those values exceed the RTTOV boundaries (temperature outside 90-400 K, surface pressure outside 400-1100 hPa, atmospheric pressure larger than 1100 hPa), the retrieval is not undertaken. In any case, such pressure or temperature would mean that the atmospheric conditions are extremely highly implausible and most probably something went wrong in the IASI level 2 retrieval.

The surface temperature being part of NOPIR retrievals, the IASI data used as a priori is not checked for specific quality, but it is clipped to the RTTOV internal boundaries of 90-400 K.

2.4 Update of the radiative transfer to RTTOV v14

The RTTOV tool has been released with a major update early 2025, with no backwards compatibility with previous versions. The new version 14 contains the latest infrared land surface emissivity atlas (CAMEL version 3) and this was considered important enough to justify updating NOPIR for the use of RTTOV v14.

However, the adaptation to this new RTTOV version was complex, as the vertical representation of the gas profiles was completely changed, from levels to layers. In addition, various options have changed their names and default values, requiring a complete cross-check of all flags and options within NOPIR. This, however, also allows to gain additional trust in the NOPIR configuration.

Comparisons to assess how this change impacts the results against the previous version are not straightforward due to the different representation of the vertical profiles, and the RTTOV documentation even states that one should not expect exact reproducibility with RTTOV versions 13 and 14 (Hocking, 2024), due to the impossibility to exactly reproduce the vertical representation.

2.5 Vertical range of the retrieval

The previous NOPIR version 1 considered only the vertical range from 800 to 80hPa. However, there is still decent sensitivity in the layers down to the surface, with a layer degree of freedom remaining similar downwards from 800hPa. It was therefore decided to update the retrieval vertical range going down to the surface. At higher altitudes than the 80hPa previous limit, the sensitivity is very low, and it would not be wise to extend the NOPIR vertical range upwards.

Considering that RTTOV 14 now works in layers and not on levels anymore, here are the NOPIR version 2 retrieval layer boundaries (in hPa, top down): 66.125, 83.231, 96.114, 110.237, 125.646, 151.266, 170.078, 200.989, 223.442, 259.969, 300.0, 358.966, 407.474, 459.712, 535.232, 596.306, 706.565, 802.371, 904.866, 1013.95

Considering altitudes down to the surface also means, obviously, that the integrated N_2O column along the retrieval range depends on the surface altitude, and that this surface altitude is accounted for when computing the column (see section 2.9).

While analysing this change in vertical representation and range, a clear bug was discovered in the retrieval. It used to keep the N_2O values below the surface for the retrieval and column calculation, therefore resulting in very weird results for areas with altitudes higher than the lowest retrieval level. This has been corrected and there are no more weird features in the N_2O columns for high altitude areas.

2.6 Sea surface emissivity

In the first NOPIR version, the surface emissivity was from the 2015 update of the data by Daniel Zhou (Zhou et al., 2011), retrieved from the IASI satellite. However, the sea surface emissivity is very well known and studied, and a model most probably gives better results than a retrieval. We therefore decided to update the sea surface emissivity to the internal RTTOV IREMIS model. This model includes the emissivity dependency with the viewing angle, which was not the case when using the Zhou emissivity. This update leads to only very minor (maximum 1%) changes in the NOPIR N_2O columns, depending on the viewing angle.

2.7 Land surface emissivity

In the first NOPIR version, the surface emissivity was from the 2015 update of the data by Daniel Zhou (Zhou et al., 2011), retrieved from the IASI satellite. Now that RTTOV contains an internal land surface emissivity atlas (Combined ASTER and MODIS Emissivity database over Land or CAMEL, Borbas et al. 2023), we decided to test it for the NOPIR retrievals.

Using the CAMEL climatology version 3 (available only since 2025 with the RTTOV version 14) versus the Zhou emissivity, we observe changes in the NOPIR N_2O integrated column, within +/-5% depending on the areas. Some previous “artefacts” over mountains and Greenland seem to be reduced using the CAMEL land surface emissivity. In addition, the root-mean-square of the spectral residuals is slightly reduced (by 0.05K) for almost all retrieval scenes, when using CAMEL. This is a clear indication that the quality of the land surface emissivity is improved, and therefore the retrieval can reproduce better the observed spectrum.

For completeness, we also tested the CAMEL climatology atlas version 2, also available in RTTOV and used in our mineral dust retrievals (MAPIR version 5.11 https://doi.org/10.18758/f7el2zbr - publication is under review). Qualitatively, the NOPIR results obtained using CAMEL v2 seem less good than those obtained with CAMEL v3. The most significant difference is when comparing day and night data. Using CAMEL v2, there are larger differences between day and night N_2O columns, which is not expected. This confirms that the newest version should be used for NOPIR.

The CAMEL atlas allows to additionally input the snow fraction, when relevant. However, we do not have this information in the IASI data and adding it would require significant work to select a data set and handle it in the retrieval. Obviously, the CAMEL climatology atlas accounts for the snow emissivity in areas where snow is usually present. To get some sense of the impact of not knowing precisely the snow cover, we tested one day retrievals with a snow fraction forced to 0.1 globally, which lead to differences only over deserts (about 1% changes in the N_2O columns). That confirms that in areas where snow is expected, the emissivity accounts for it even if the snow fraction is not provided, while in areas where snow is never observed, snow fraction may have an impact on the CAMEL land surface emissivity, but these events should not occur.

Finally, RTTOV contains an option to account for the land surface emissivity dependence with the viewing angle. We tested it and it leads to very small changes in the NOPIR retrieval results, all pointing to a plausible improvement when using the emissivity angle correction: no change in residual or degrees of freedom, and very small changes in N_2O columns (maximum +/- 0.5%). The clear change is for the retrieved surface temperature, especially over deserts: it seems more continuous when using the angle correction. This is purely qualitative, and would be very difficult to validate, but it points to a slight improvement when using the angle correction, which is also the expected behaviour. We therefore selected that option.

2.8 A priori N_2O profiles

NOPIR in its first version uses a monthly GEOS-Chem (Wells et al., 2015) climatology based on latitude band averages. This concept of latitude band average was re-analysed during the current work, because it might not properly represent the profile for different surface altitudes within a latitude band. NOPIR version 2 now uses a monthly GEOS-Chem climatology, on the 4° lat x 5° lon GEOS-Chem grid. The profiles are spatially linearly interpolated from that grid to each IASI observation geolocation, to avoid discontinuities.

This results in +/-2.5 ppb in the N_2O concentration in the highest layers of the retrieval, where the sensitivity is lowest and therefore the a priori has the strongest impact. However, the total N_2O column over the retrieval range changes no more than 0.25%.

2.9 Column and column uncertainty calculations

With the update in RTTOV from version 13 to version 14, the concept of the vertical profile was changed from levels to layers. Therefore, the computation of the N_2O column from the profile also needed to be updated. In the first NOPIR version, the column computation was done by calculating the altitude grid (in km), converting the N_2O dry volume fraction to concentration, and integrating vertically. In NOPIR version 2, we designed an operator to do the unit conversion and layer summation, which can then be applied to both the vertical profile and the uncertainty covariances matrices.

The operator L has the same size as the vertical profile and is written as:

$$L = N_A * 10^{-4} * dpi/(g * Mair) * (1 - H_2O * 10^{-6}) * 10^{-6}$$

Where N_A is the Avogadro number, the 10^{-4} factor converts it to the units of molecules/cm^2 used for the column reporting, dpi is the pressure depth of the layers in Pa (starting from the surface pressure and set to 0 for layers below the surface), Mair is the moist air molar mass (calculated using the H_2O vertical profile), and the two multiplications by 10^{-6} account for the fact that the gas volume mixing ratios are expressed in ppm in the retrieval and in RTTOV. This operator is specific to each IASI pixel / retrieval.

The column (N_2O or H_2O) is obtained from the profile simply with: $\sum(\mathrm{L.dot(profile)})$

The absolute uncertainty on the column is obtained from the uncertainty covariance matrix S with: $\sqrt{\mathrm{L.dot(S).dot(L}^T))}$

The NOPIR retrievals provide uncertainty covariance matrices for propagation of the spectral noise, for the vertical smoothing, and for the propagation of the uncertainty on the temperature and humidity profiles. The total uncertainty covariance matrix is obtained by summing all these. This has not changed with respect to the first algorithm version.

2.10 Digital elevation model

NOPIR version 1 used the surface altitude available in the IASI data. However, it was discovered that for the IASI-C data, the surface altitude is sometimes missing, which makes the retrieval collapse. Therefore, we updated the surface altitude to use a digital elevation model. The latter is built on ASTER version 003 (NASA, 2018) data where available (83°S to 83°N latitude) and completed using the Reference Elevation Model of Antarctica (REMA) v2 (Howat et al., 2022) for Antarctica. The source data has extremely high horizontal resolution, which is not necessary for our purposes and difficult to handle. It was therefore transferred to a 0.25-degree grid, averaging the elevation within each grid cell.

2.11 NOPIR quality control

The quality control after NOPIR retrievals has not changed but is worthy to be mentioned anyway. The following criteria must be met for the retrieval to be considered good:

- Convergence of the retrieval within a maximum of 10 iterations
- Root-mean-square of the spectral residuals <0.2K
- Individual retrieval channel spectral residuals <0.4K
- Minimum 0.75 degree of freedom
- Retrieved surface temperature between 200 and 350K
- Dust Aerosol Optical Depth at 10µm (from MAPIR version 5.11 https://doi.org/10.18758/f7el2zbr) <0.25 (even though the spectral retrieval window is completely different from the dust retrieval window, it was shown with version 1 that there is a significant impact of the dust presence on the NOPIR retrievals)

3 Quick look at some results, comparison with version 1

In this section, we will show some results from NOPIR versions 1 and 2, which highlight the changes. As the lower boundary for the two versions of the retrievals is different (800 hPa for version 1 and down to the surface for version 2), a direct comparison of the column is of course difficult. Figure 3 shows the digital elevation model used in NOPIR, as an aid in understanding the patterns in N_2O columns. With NOPIR version 2, one expects lower values of the N_2O column with increasing surface altitude.

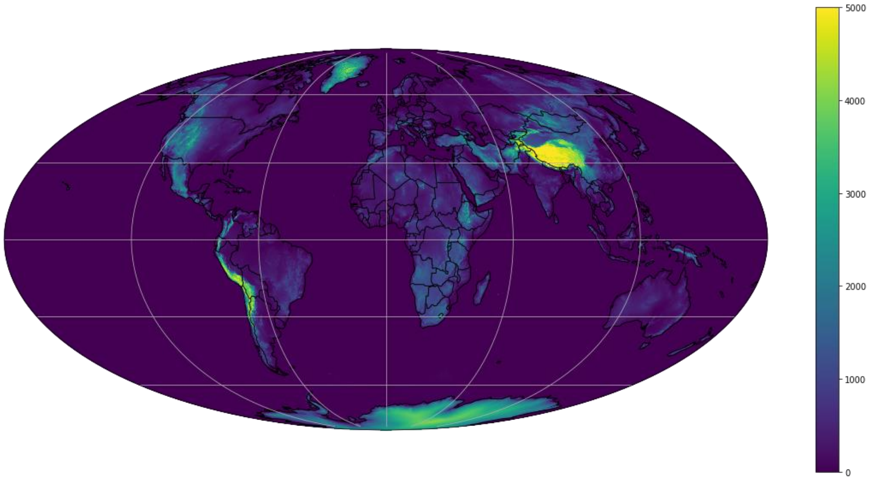

Figure 3: surface elevation map

3.1 15 March 2020

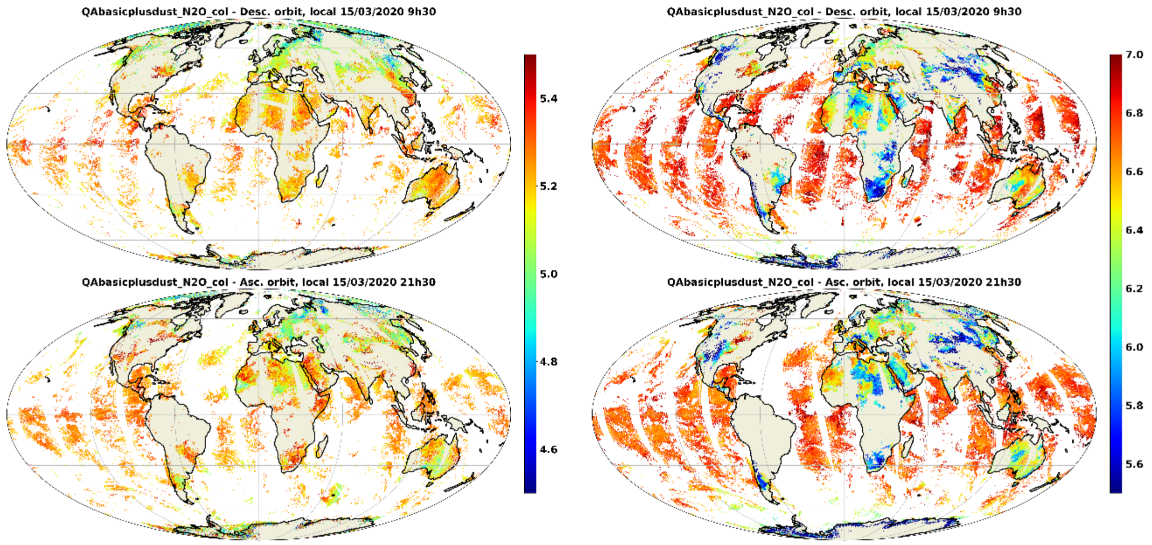

Figure 4: 15 March 2020, N_2O integrated column along the NOPIR retrieval vertical range; (left) version 1, levels at 800 to 80hPa; (right) version 2, layers covering from the surface to 66hPa; (top) 9h30 local solar time; (bottom) 21h30 local solar time. Note the different colour scales for the two algorithm versions.

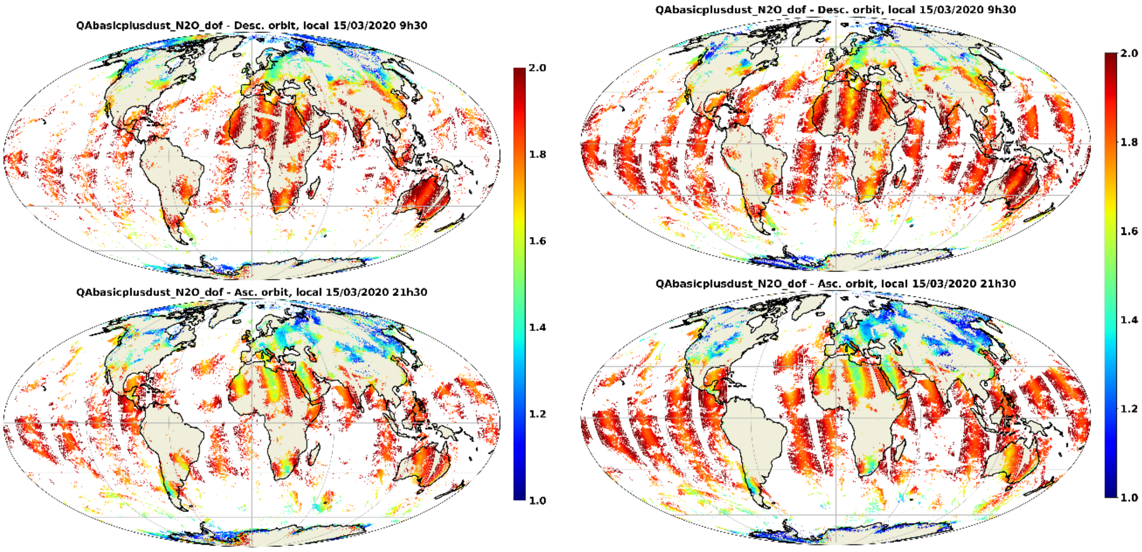

Figure 5: 15 March 2020, number of degrees of freedom in NOPIR retrievals; (left) version 1; (right) version 2; (top) 9h30 local solar time; (bottom) 21h30 local solar time

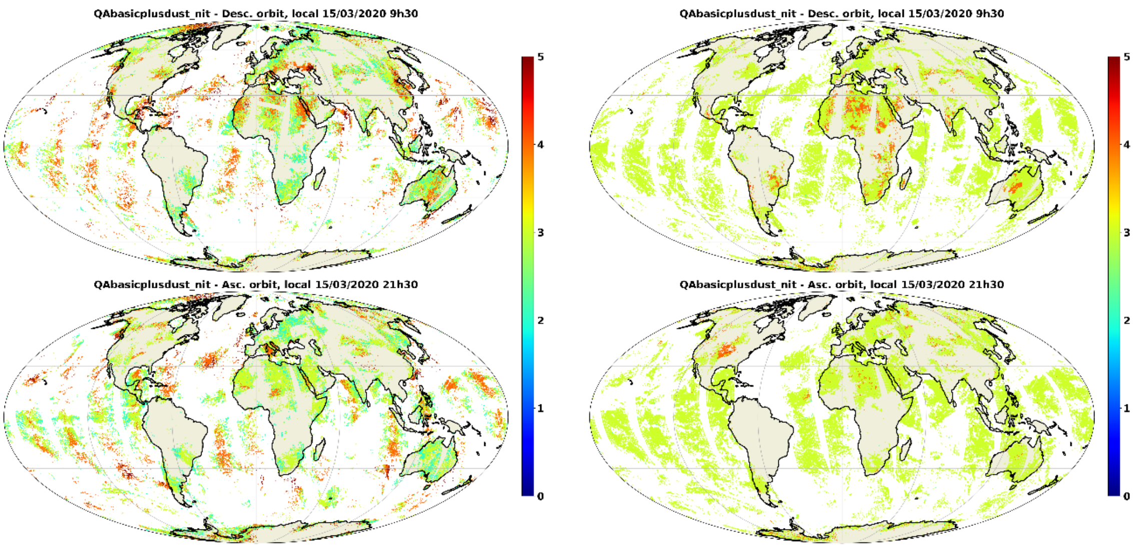

Figure 6: 15 March 2020, number of iterations in NOPIR; (left) version 1; (right) version 2; (top) 9h30 local solar time; (bottom) 21h30 local solar time

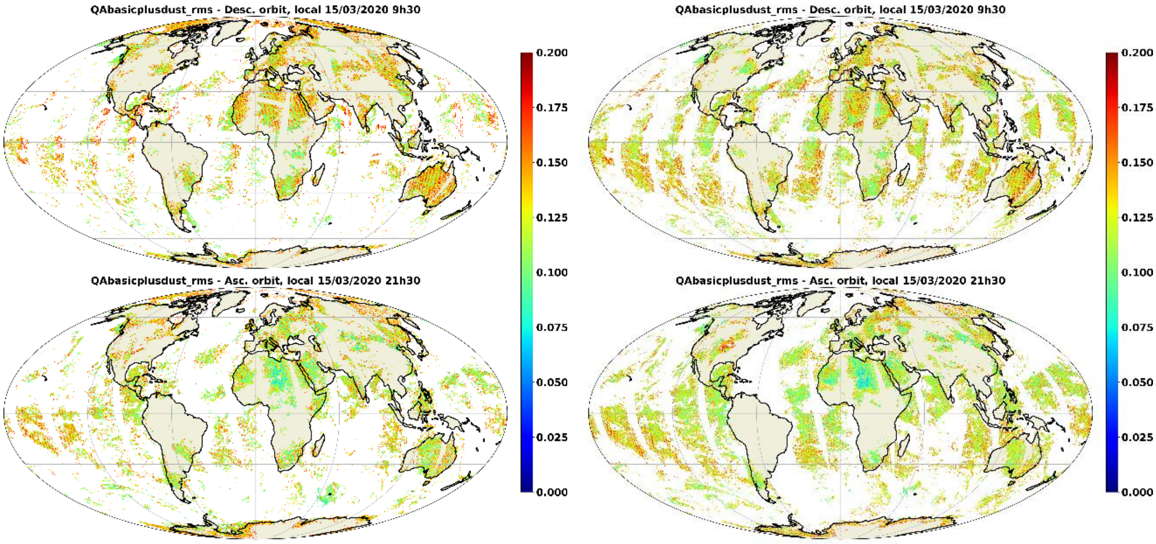

Figure 7: 15 March 2020, root-mean-square of spectral residuals in NOPIR; (left) version 1; (right) version 2; (top) 9h30 local solar time; (bottom) 21h30 local solar time

3.2 21 September 2020

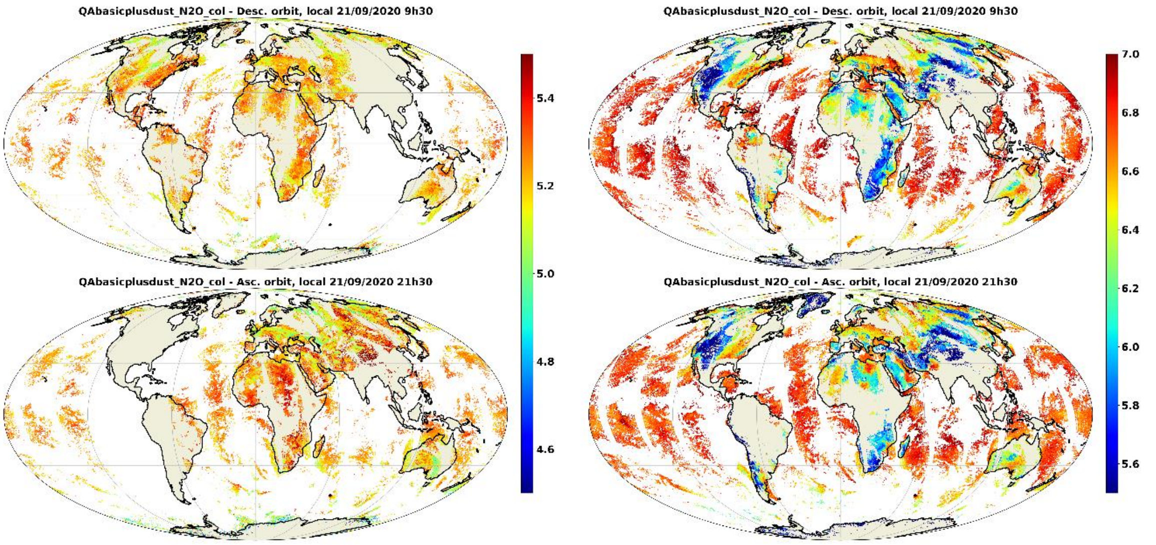

Figure 8: 21 September 2020, N2O integrated column along the NOPIR retrieval vertical range; (left) version 1, levels at 800 to 80hPa; (right) version 2, layers covering from the surface to 66hPa. Note the different colour scales; (top) 9h30 local solar time; (bottom) 21h30 local solar time.

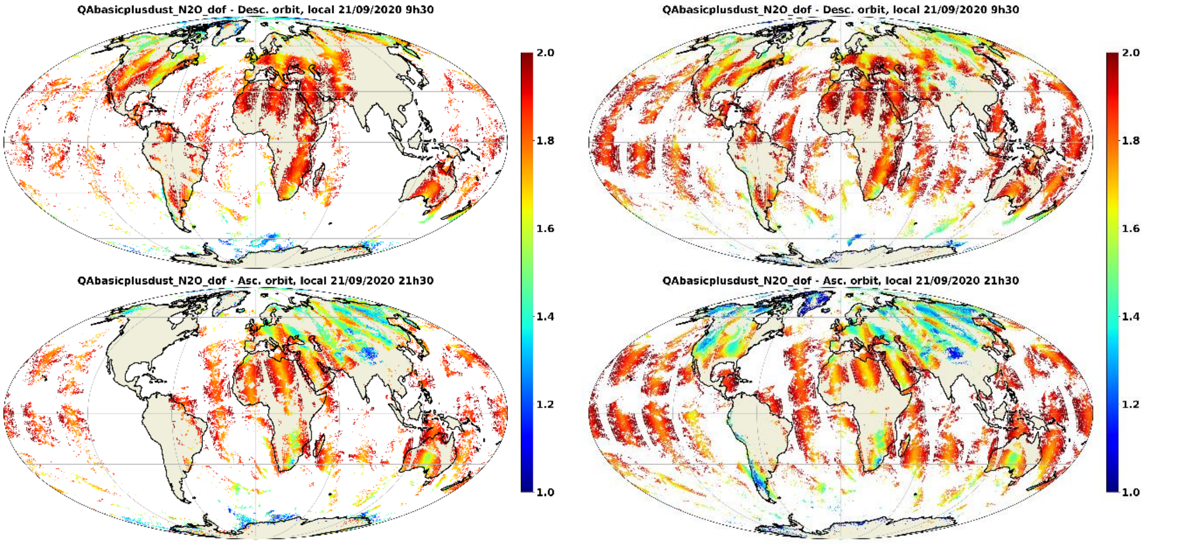

Figure 9: 21 September 2020, number of degrees of freedom in NOPIR retrievals; (left) version 1; (right) version 2; (top) 9h30 local solar time; (bottom) 21h30 local solar time

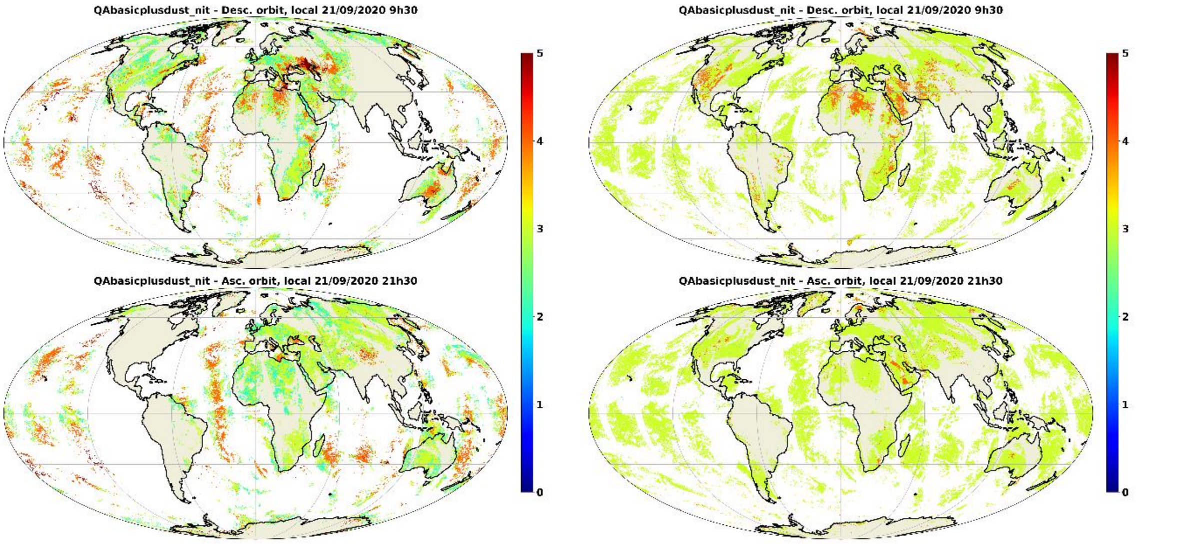

Figure 10: 21 September 2020, number of iterations in NOPIR; (left) version 1; (right) version 2; (top) 9h30 local solar time; (bottom) 21h30 local solar time

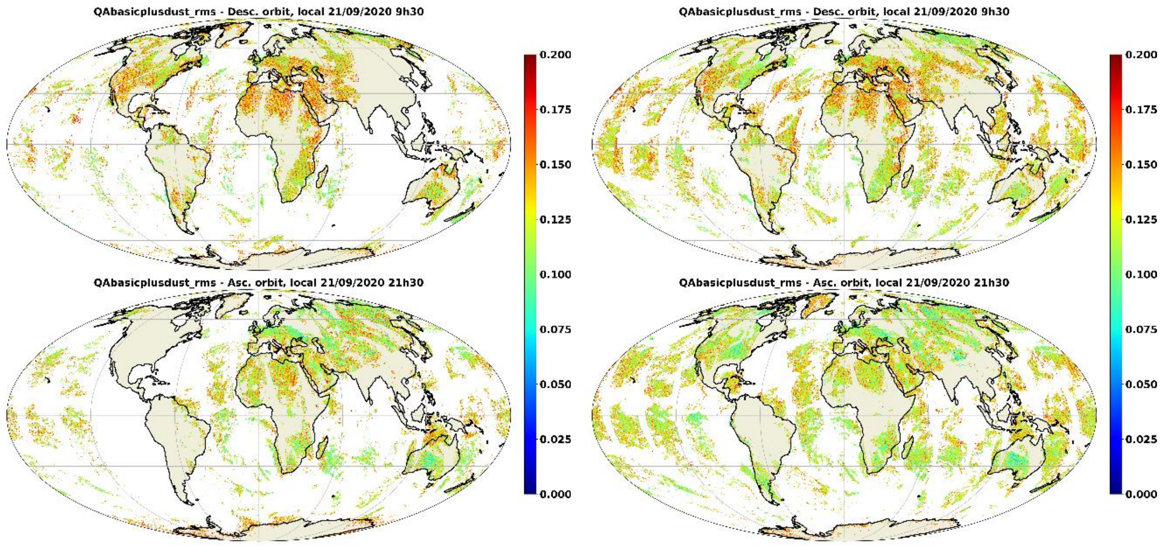

Figure 11: 21 September 2020, root-mean-square of spectral residuals in NOPIR; (left) version 1; (right) version 2; (top) 9h30 local solar time; (bottom) 21h30 local solar time

3.3 Short discussion

Figure 4 to Figure 7 show respectively the N_2O column, degrees of freedom, number of iterations and retrieval spectral residuals for NOPIR version 1 (left in each plot) and version 2 (right in each plot), for 15 March 2020. Figure 8 to Figure 11 show the same plots for 21 September 2020. In all cases, the top plot shows the data for IASI local morning (about 9h30 local solar time) observations, while the bottom plot shows observations for local evening (about 21h30 local solar time).

The N_2O columns are integrated along the retrieval range, which differs in the two versions, and are therefore not to be compared in absolute values. However, we can compare patterns and coverage for these specific dates. NOPIR version 2 shows a N_2O column clear dependency with the surface altitude, with lower N_2O columns when the surface is higher, which is expected as the retrieval goes down to the surface. In version 1, there were some strange artefacts of high N_2O columns mostly (but not only) at high altitude areas. Those are not present any more in version 2. Version 2 also shows a better spatial continuity in the N_2O columns than version 1, and less “noise”. This could partly be due to the more consistent reprocessed data (IASI level 2 PWLR3 is also less noisy than OE), and to the change in surface emissivity.

The daily coverage is different between the 2 versions, with version 2 offering overall better coverage.

The total number of degrees of freedom is mostly similar for both versions and shows a dependence with the viewing angle as expected (larger angles mean a longer atmospheric path and therefore increased sensitivity).

The number of iterations in the retrievals is more stable in version 2, with 3 iterations in most cases. Version 1 showed patterns over ocean, with the number of iterations depending on the satellite viewing angle. This is not expected and could reflect the surface emissivity dependence with the viewing angle, which was not accounted for in version 1.

Finally, the retrieval spectral residuals are, in general, slightly lower in version 2, resulting in more cases passing the quality check and improving the spatial coverage.

4 Quick look at IASI-A versus IASI-C continuity

The NOPIR retrieval algorithm applied to both instruments' data is exactly the same. The input data from IASI-A and IASI-C is however different in format and partly in contents, as detailed in sections 2.2 and 2.3. All variables necessary were selected with the highest consistency in mind, wherever possible. Full consistency between NOPIR results from both instruments is therefore expected.

Metop-A has started drifting from its reference orbit in August 2016 (equator crossing time of about 9:30), after its last manoeuvre. This drift remains very small until 2018 (equator crossing time is about 9:15 at the end of that year), but starts to be significant during the year 2019, with the equator crossing time of about 8:50 at the end of the year, then about 8:25 at the end of 2020 and about 8:00 when IASI-A was decommissioned. Atmospheric N_2O concentration does not bear a diurnal cycle, but the IASI level 2 data used as input for NOPIR (especially the temperature profiles) may be of altered quality when the drift becomes significant.

The long-term analysis reveals significantly different trends when using full time series of IASI-A or IASI-C, or both combined. **Error! Reference source not found.** shows examples of such analysis for two locations, highlighting that in some cases (as the first one) the two data sets seem consistent, and the linear trends are within the uncertainty of each other. For other locations (such as the second one), there are significant differences in those trends.

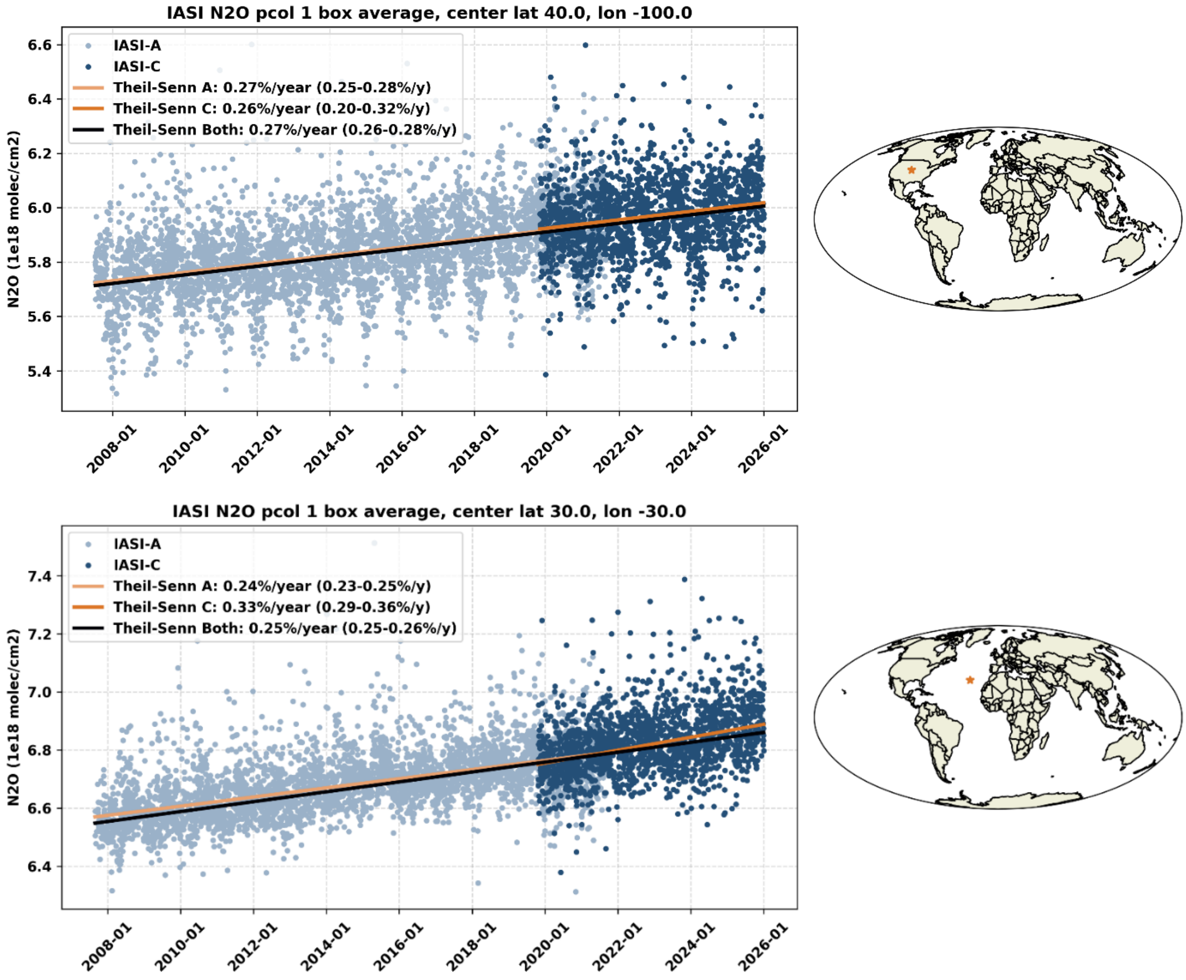

Figure 12: Examples of IASI-A and IASI-C NOPIR v2.1 linear trends in N2O partial column (along the retrieval vertical range) for two geographic locations (1 degree average in latitude and longitude around the marked point).

The overlap period between both instruments (October 2019 to August 2021) was therefore analysed globally (daily data, 1 degree latitude / longitude grid), in terms of bias, variance ratio, correlation and P-value for the hypothesis that the two datasets are samples from the same distribution. As Figure 13 shows, a mean bias of up to 1% exists between the integrated N_2O columns from IASI-A and IASI-C, with clear geographical patterns. The noise in the NOPIR data is also different for the two instruments, with again clear geographical patterns. The Pearson correlation coefficient between the two datasets is very low, which can be linked to the fact that, in general, the NOPIR time series are relatively noisy while the expected changes are very small, especially during the short overlap period. Finally, the hypothesis that the IASI-A and IASI-C NOPIR samples are samples of the same distribution is invalid in many geographic areas (in red in the figure). The geographical patterns however suggest that indeed the temperature profiles play a role in these IASI-A versus IASI-C differences, therefore pointing to the plausible role of the Metop-A drift.

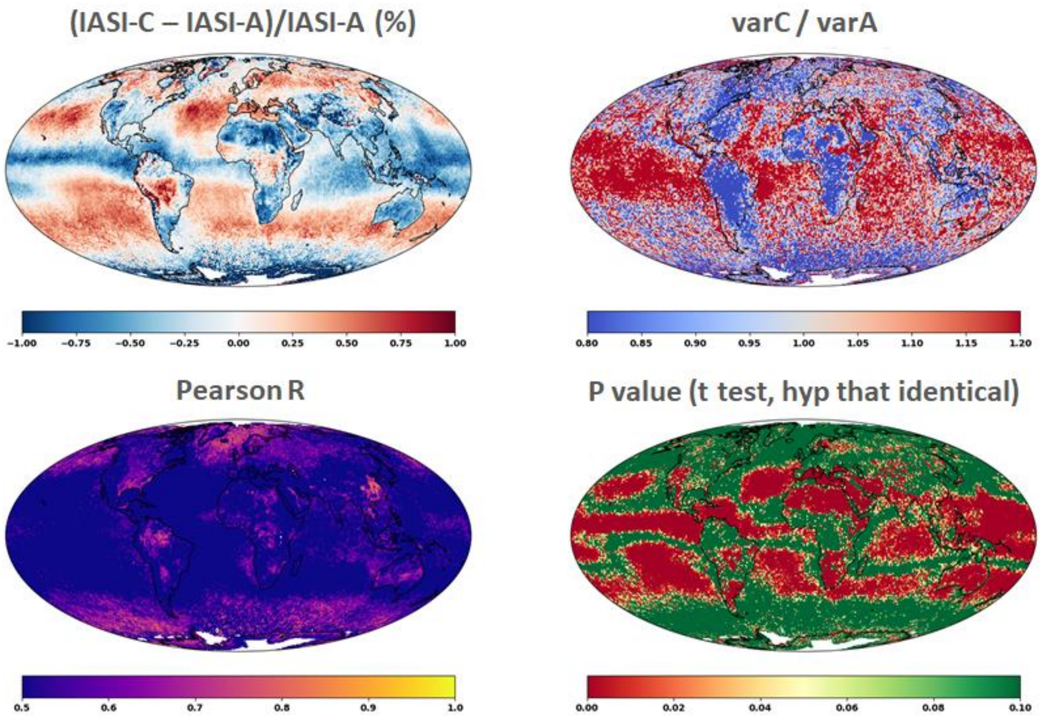

Figure 13: statistical analysis of the IASI-A and IASI-C overlap period (October 2019 to August 2021), daily data on a 1 degree latitude / longitude grid

If making the hypothesis that the IASI-A data becomes of a lesser quality end of 2019, a long-term time series may be constructed using IASI-A until the start of IASI-C operational data on 24 October 2019, then continue the time series with IASI-C data. Doing that, we lack the possibility to cross-check instrument consistency, which would then require processing IASI-B for some overlap time with both instruments. For the best consistency between linear trends, one should only use full years of data, therefore IASI-C from November 2007 to October 2019, then IASI-C from November 2019 to October 2025.

The produced full time series are more consistent (see Figure 14), with the same linear trend extracted using only IASI-A or using both data-sets, pointing to a constant increase rate for N_2O. The trends obtained with only IASI-C are different, but this may be attributed to the much shorter time series. However, there remain locations where the trends are inconsistent (not within uncertainty of each other) even with the above-mentioned precautions. The N_2O series at those locations seem noisier, which could be a reason for inconsistency. It may also reflect a real change in the N_2O increase rate. More analysis would be required to confirm this preliminary assessment that a full time series should be constructed using IASI-A only until IASI-C starts to provide data, then switch.

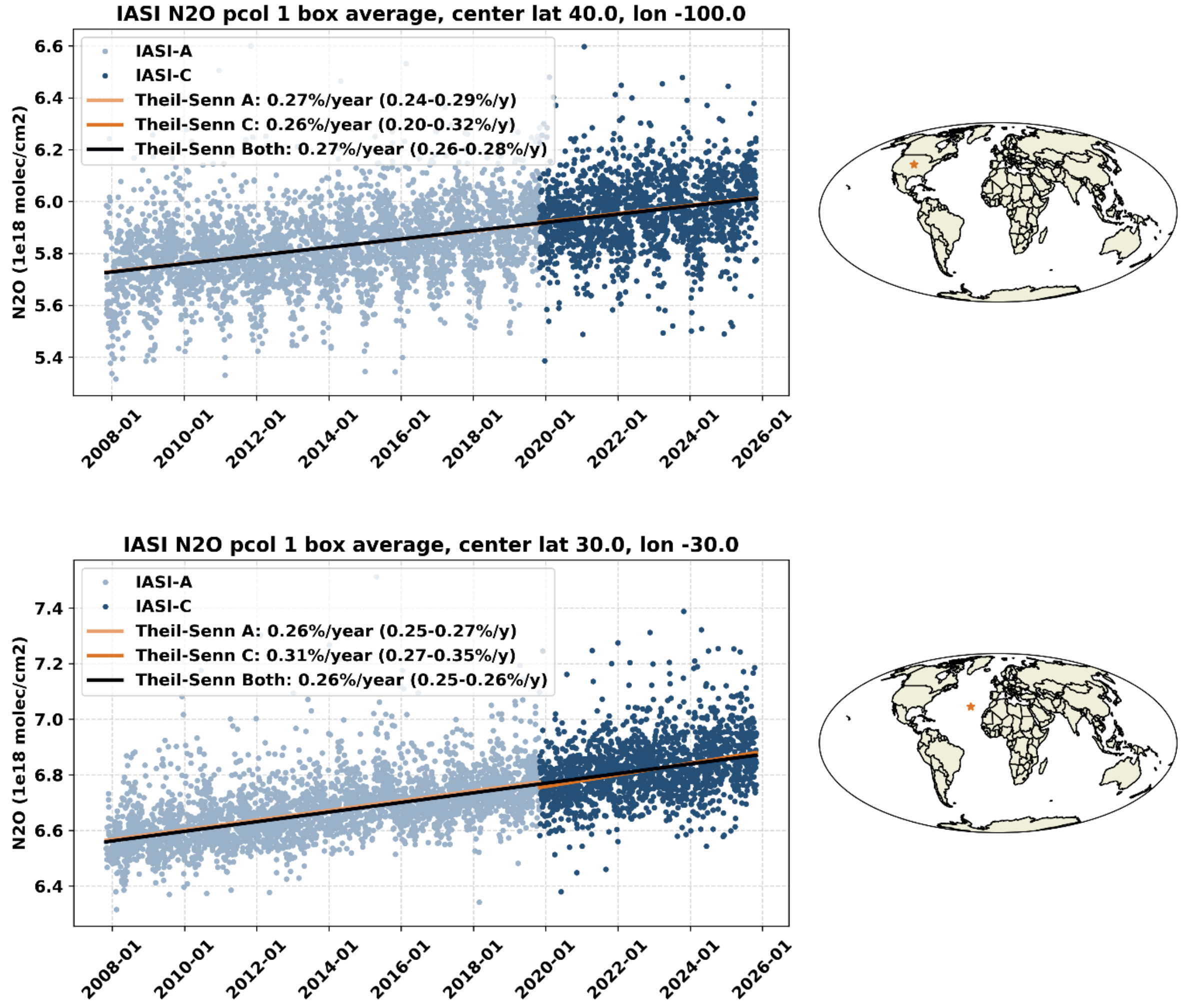

Figure 14: same as Figure 12, but using IASI-A from Novembre 2007 to October 2019, and IASI-C from Novembre 2019 to October 2025

5 Conclusions

The most important goal of this work was to obtain long-term consistent N_2O data from IASI using the NOPIR algorithm, allowing to derive climate trends. This is achieved for IASI-A by using the reprocessed IASI data as input, and for IASI-C by selecting from the available data those that are the most consistent possible with the IASI-A reprocessed data.

In addition, before a full-time series reprocessing, it was wise to address some issues discovered in the NOPIR version 1 data and test some retrieval improvements. The largest issue in NOPIR version 1 was an unexpected high N_2O column in high-altitude areas. Solving that took a lot of testing and debugging, which was also interesting as many retrieval parameters were re-tested and confirmed in their original choices, overall consolidating the approach. Finally, the identified issue was due to a misconsideration of the surface altitude in defining the N_2O profile within the retrieval, while it was correctly defined in the radiative transfer. NOPIR version 2 no longer contains high columns over high-altitude areas.

The opportunity to update to the latest RTTOV version 14 (available early 2025) was also taken, and it was a challenge to implement because the layer and level definitions were totally modified, while many options and default values were updated. However, it was worth the work as it also opened the possibility to use the latest land surface emissivity database, which should contribute to the overall improvement of NOPIR results.

Another important change is the extension of the vertical range of the profiles down to the surface. That, together with the modified vertical representation, renders difficult the direct comparison of absolute N_2O columns from the two versions.

Finally, the a priori handling was improved from a latitudinal climatology to a gridded climatology, and the uncertainty analysis is better handled, although the principles remain the same.

These changes in the retrieval have shown to improve significantly the NOPIR data quality, removing any previously observed weird artefacts and, at the same time, improving the validation statistics (not shown here).

The complete time series of IASI-A and IASI-C have been processed and delivered. Initial validation results (not shown here) highlight a good quality of the data with respect to reference datasets, for both IASI instruments separately. However, the initial analysis to derive trends shows discrepancies in the results obtained considering both instruments together. The statistical analysis of the data during the overlap of the two instruments shows significant differences, which are most probably linked to the drifting orbit of Metop-A becoming significant end 2019.

A preliminary assessment shows that merging the two time series should best be undertaken using IASI-A data until end October 2019 then switching to IASI-C. Confirmation of the full consistency between both data sets should however still be provided, for which using IASI-B seems the best option.

References

Borbas, E. E., Hulley, G., Loveless, M., Knuteson, R., and Hook, S.: The Combined ASTER and MODIS Emissivity database over Land (CAMEL) Version 3 Algorithm Theoretical Basis Document and Users' Guide, 2023

EUMETSAT, Validation Report IASI Level2 T and Q profiles release 1, EUM/OPS/DOC/19/1091375, 2021, https://doi.org/10.15770/EUM_SEC_CLM_0027

Hocking, J.: RTTOV v14 User Interface Changes, 2024, NWPSAF-MO-UD-056

Hocking, J.: RTTOV v14 Users' Guide, 2025, NWPSAF-MO-UD-055

Howat, Ian, et al., 2022, The Reference Elevation Model of Antarctica - Mosaics, Version 2, https://doi.org/10.7910/DVN/EBW8UC, Harvard Dataverse, V1

NASA/METI/AIST/Japan Spacesystems, and U.S./Japan ASTER Science Team. ASTER Global Digital Elevation Model V003. 2018, distributed by NASA EOSDIS Land Processes DAAC, https://doi.org/10.5067/ASTER/ASTGTM.003

Vandenbussche, S., Langerock, B., Vigouroux, C., Buschmann, M., Deutscher, N. M., Feist, D. G., García, O., Hannigan, J. W., Hase, F., Kivi, R., Kumps, N., Makarova, M., Millet, D. B., Morino, I., Nagahama, T., Notholt, J., Ohyama, H., Ortega, I., Petri, C., Rettinger, M., Schneider, M., Servais, C. P., Sha, M. K., Shiomi, K., Smale, D., Strong, K., Sussmann, R., Té, Y., Velazco, V. A., Vrekoussis, M., Warneke, T., Wells, K. C., Wunch, D., Zhou, M., and Mazière, M. D.: Nitrous Oxide Profiling from Infrared Radiances (NOPIR): Algorithm Description, Application to 10 Years of IASI Observations and Quality Assessment, 30, https://doi.org/10.3390/rs14081810, 2022.

Wells, K.C.; Millet, D.B.; Bousserez, N.; Henze, D.K.; Chaliyakunnel, S.; Griffis, T.J.; Luan, Y.; Dlugokencky, E.J.; Prinn, R.G.; O'Doherty, S.; et al. Simulation of atmospheric N2O with GEOS-Chem and its adjoint: Evaluation of observational constraints. Geosci. Model Dev. 2015, 8, 3179–3198. doi:10.5194/gmd-8-3179-2015

Zhou, D.; Larar, A.; Liu, X.; Smith, W.; Strow, L.; Yang, P.; Schlüssel, P.; Calbet, X. Global Land Surface Emissivity Retrieved from Satellite Ultraspectral IR Measurements. Geosci. Remote Sens. IEEE Trans. 2011, 49, 1277–1290. Available online: https://doi.org/10.1109/TGRS.2010.2051036

***** End of Document *****